UCRL- 93497
PREPRINT

TIBER--Tokamak Ignition/Burn Experimental Research

C. D. Henning, B. G. Logan,
W. L. Barr, R. H. Bulmer, J. N. Doggett,
B. M. Johnston, R. W. Hoard, J. D. Lee,
J. R. Miller, and D. S. Slack

This paper was prepared for submittal to
11th Symposium on Fusion Energy,
Austin, TX, November 18-22, 1985

November 1985

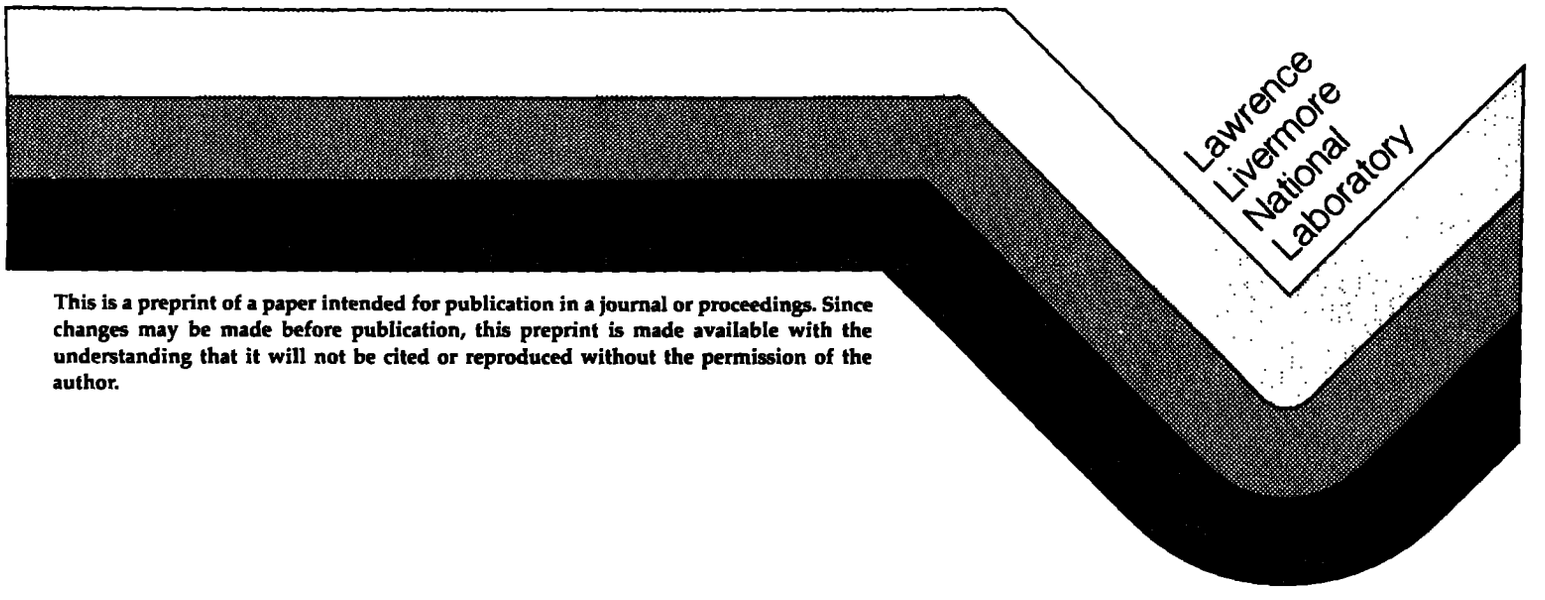

TIBER - TOKAMAK IGNITION/BURN EXPERIMENTAL RESEARCH*

C. D. Henning, B. G. Logan, W. L. Barr, R. H. Bulmer, J. N. Doggett,
B. M. Johnston, R. W. Hoard, J. D. Lee, and D. S. Slack

Lawrence Livermore National Laboratory
Livermore, CA 94550

J. H. Shultz

Massachusetts Institute of Technology
Cambridge, MA

Abstract

As part of a continuing effort by the Office of Fusion Energy to define an ignition experiment, a superconducting tokamak has been designed with thin neutron shielding and aggressive magnet and plasma parameters. By so minimizing the inner radial dimensions of the tokamak center post, coil, and shielding region, the plasma major radius is reduced, with a corresponding reduction in device costs. The peak nuclear-heating rate in the superconducting TF coils is 22 mW/cm^3, which results in a steady heat load of 50 kW to the cryogenic system. Fast-wave, lower-hybrid heating would be used to induce a 10-MA current in a moderate density plasma. Then pellet fueling would raise the density to achieve ignition as the current decays in a few hundred seconds. Steady-state current drive in subignited conditions permits a 0.8 MW/m^2 average wall loading to study plasma and nuclear engineering effects.

Introduction

The Tokamak Ignition/Burn Experimental Research (TIBER) device is the smallest superconducting ignition tokamak design to date. To reduce the size and cost of the tokamak, we had to make a number of aggressive design assumptions. For example, plasma shaping is used to achieve a high plasma beta (the ratio of plasma pressure to magnetic field pressure). In addition, neutron shielding is minimized by radiation hardening of the magnets[1] to achieve the desired small device size (major radius of 2.6 m, plasma height of about 0.8 m). However, the superconducting toroidal-field magnets must still be shielded sufficiently to reduce the neutron heat load and the gamma-ray dose to various components of the device. In particular, the insulation must retain adequate strength and electrical properties after irradiation to very high end-of-life neutron fluences (greater than 10^{19} neutrons/cm^2) and gamma-ray doses (above 10^{10} rads), especially in those portions of the magnet adjacent to the shield penetrations required for diagnostics and plasma-heating systems. For TIBER, the peak fusion heating rate in the superconducting toroidal-field coil is calculated to be 22 mW/cm^3, for a total system heat load of 50 kW.

A high-field (14-T) plasma-shaping coil is used in the usual ohmic heating coil position. By shaping the plasma profile with the coil to produce a modest indentation, we achieve a plasama beta of 10% in the first stability regime (about twice that normally achieved in a tokamak). All inner-radius components of the tokamak must be kept as small as possible so that the plasma major radius can be minimized and plasma shaping can be maximized. Accordingly, high magnet current densities of 4 kA/cm^2 and an integrated structural design are required.

Noninterlinking toroidal- and poloidal-field coils are used in TIBER to permit easy maintenance. The entire device is enclosed in a single vacuum vessel, similar to that on the Magnetic Fusion Test Facility at LLNL. This allows us to minimize the internal dimensions of the tokamak and to provide easily serviced external vacuum joints for rapid disassembly. Full shielding of the magnet systems is achieved with fitted shield modules that are accessible for maintenance and repair without magnet removal.

We envision the use of fast-wave, lower hybrid radiofrequency heating to induce a plasma current of 9.7 MA at a low plasma density of about 0.4×10^{14} ions/cm^3. A laser-driven pellet fuel injector would raise the plasma density to 3×10^{14} ions/cm^3, with continued fast- and slow-wave lower hybrid heating to achieve ignition. Because the current drive is not efficient at high plasma density, the current would decay in a few hundred seconds. During this period, we would turn off all plasma heating so as to study pure ignition physics. As the plasma current decays to 7.4 MA and the plasma density drops to 10^{14} ions/cm^3, slow-wave lower hybrid heating would again be used to sustain a steady-state plasma with an average wall loading of 0.8 MW/m^2 and a peak at the outside leg of 2.1 MW/m^2. Thus, the TIBER device can be used to study ignition physics and, when operating in a steady-state, current-driven mode, to study plasma-wall interactions, helium ash removal, and neutron damage effects.

Design Description

A point design of the TIBER device is summarized in Table I. The confinement scaling used for the TIBER operation shown in Fig. 1 is separated into different scalings for ions and electrons. The electron confinement is taken to be neoalcator, $\chi_e = 1.5\, f_e a\sqrt{\kappa}/(R^2 n_{20})$, where f_e is an anomaly factor to account for high beta deterioration ($f_e = 2$ is used). The ion confinement is taken to be neoclassical

$$\chi_i = 4.1 \times 10^{-2}\, f_i (R/a\sqrt{\kappa})^{3/2} \langle q\rangle^2\, n_{20}/(B_t^2\, T_{10}^{1/2})$$

$$\langle \beta_t \rangle < 0.04\, \frac{I_p(\mathrm{MA})}{a B_t(\mathrm{T})}\ ,$$

where f_i is an anomaly factor ($f_i = 2$). Using the Troyon-Wesson beta limit the ignition condition is

This work was performed under the auspices of the U.S. Department of Energy by the Lawrence Livermore National Laboratory under contract number W-7405-ENG-48.

Table I. TIBER reference case parameters.

Fixed parameters

Major radius R = 2.60 m		Toroidal field B_T = 5 T	
Minor radius a = 0.73 m		Fractional radiation losses($1 - f_\alpha$) = 0.2	
Aspect ratio A = 3.6		Ion confinement: Neoclassical/2	
Elongation	1.94	Electron confinement: Neoalcator/2	
Triangularity	0.60		
Indentation	0.05	Beta: 0.04 $I_p/(a\ B_T)$	

Variable parameters	Pulsed ignition mode	Steady state current drive mode
Plasma current, I_p(MA)	9.7	7.4
Ave. toroidal beta, β_T(%)	10.6	8.1
Ignition margin, M	1.5	0.60
Ion/electron transport, χ_i/χ_e	1.1	0.1
Ion temperature, T_i(keV)	10	30
Electron temperature, T_e(keV)	10	24
Ave. edge safety factor, q_e	2.2	3.2
Neutron wall load, Γ_n(peak) (MW/m^2)	4.0 (1.6 ave)	2.1 (0.8 ave)
Fusion power, P_{fusion}(MW)	440	222
Ave. density, n (10^{20} m^{-3})	3.3	0.94
Current drive, P_{cd}(MW)	0	22.4

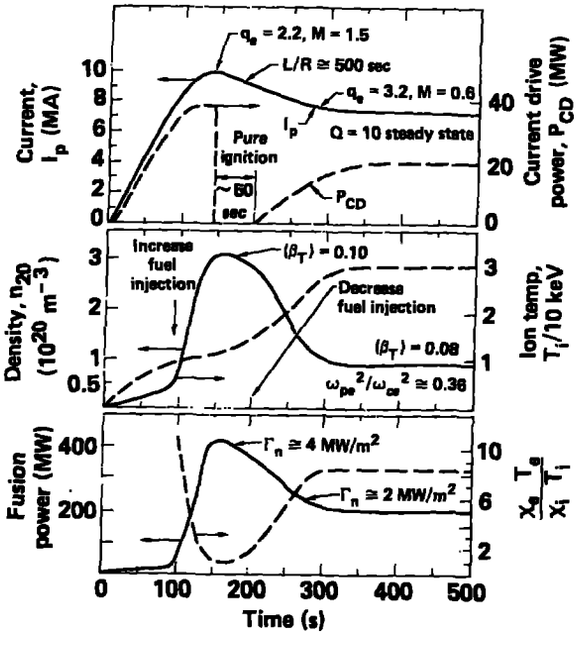

Figure 1. Both pure ignition and high-Q steady-state physics can be explored in a Mission II device.

$$I_p^2 \geq \frac{938\ M_{eff}\ a\ T_{10}\left(\frac{\chi_i}{\chi_e} + \frac{T_e}{T_i}\right)\left(1 + \frac{T_e}{T_i}\right)^2 f_e}{R^2\ B_T^2 \sqrt{\kappa}\ f_\alpha\ [\sigma v_{corrected}]} \ .$$

where M_{eff} is the ignition margin. During the 50-s high-density, pure-ignition period in Fig. 1, $M_{eff} > 1.5$ and $T_e/T_i \simeq 1$. During the steady-state current drive (t > 300 s in Fig. 1), $M_{eff} = 0.6$ and $T_e/T_i \simeq 0.8$ result from the high temperatures, with the current drive power input augmenting the alpha heating. The current-drive power input P_{cd} is calculated from Karney and Fisch:[2]

$$P_{cd} = 2.78\ \frac{I_p(MA)\ R(m)\ n_{20}}{\left[1 + \left(\frac{T_{10}}{2.5}\right)^{1.16}\right]} \ ,$$

where the denominator is a fit to Karney and Fisch curves for current drive efficiency, taking into account favorable relativistic effects at high T_e, and averaged over parallel indexes η = 1.5 to 2.0.

Laser-Driven Pellet Injector

To minimize plasma-wall interactions such as sputtering, to reduce DT gas recycling near the wall, and to mitigate tritium flows in the vacuum system, deep pellet fueling would be desirable for TIBER. In addition, with deep fueling it may be possible to increase density and $n\tau$ beyond normal Murakami limits (Alcator-pellet results) if the pellets penetrate half-way or more to the axis. Also, the net outward particle transport flux due to the deep fueling may generate an appreciable bootstrap current. To obtain deep fueling, however, requires pellet velocities much greater than the 1 km/sec velocities available with pneumatic drives, especially when the effects of fast alpha heating of the pellet are taken into proper account. Lasers and rail guns have previously been proposed to obtain higher pellet velocities, but the poor mechanical strength of DT ice limits the maximum acceleration "g" forces unless one allows the pellet to disintegrate (even vaporize and ionize) and expand at sound speed transverse to the direction of pellet acceleration. Here we will use a laser-ablation driven pellet plasma injection scheme[3] shown in Fig. 2.

A conventional DT ice pellet pneumatic injector fires pellets at the rate of 10 pellets per particle confinement time (3 Hz), with each pellet large enough to deposit 10% of the plasma inventory. Just as the ice pellet arrives at the separatrix between the confined plasma and the scrape-off layer, traveling at a speed of 1 km/sec, a laser beam is fired to drive the back of the pellet. At laser intensities of 5×10^{12} watts/cm² (10 to 100 times lower intensity than those in inertial fusion experiments today, but 10 to 100 times higher than the intensity that would otherwise be limited by the strength of the DT ice) the laser prepulse is sufficient to shock-heat the ice pellet to 5 eV preheat temperature, whereupon the main laser pulse interacting at the critical plasma density layer generates several megabars of ablation pressure, accelerating the pellet to velocities on the order of 50 km/sec in a pulse length of order $r_0\sqrt{T_0}/m \simeq$ 70 nsec, where r_0 is the characteristic "payload" pellet plasma radius at the preheat temperature T_0, and at a pellet plasma density roughly equal to the equivalent solid density $n_0 \simeq 6 \times 10^{22}$ cm^{-3}. The payload plasma radius r_0 is somewhat smaller than the initial DT ice pellet radius because of the mass lost in ablation (typically 25 to 50% less mass in the payload), and the laser pulse length is limited to the time it takes for the critical plasma density layer to "burn through" the pellet plasma expanding spherically at the preheat sound speed $\sqrt{T_0/m_i}$. Since the center-of-mass of the pellet plasma is accelerated forward to a velocity $V_F > \sqrt{T_0/m_i}$, the pellet plasma sweeps forward as an expanding plume with an initial 30 to 35 degree half cone angle. The pellet plasma initial

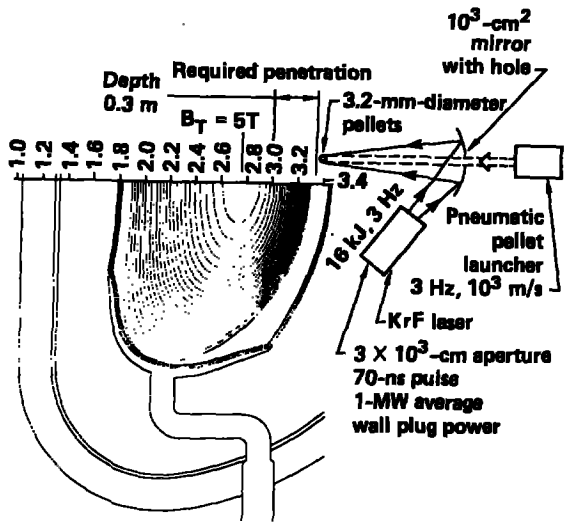

Figure 2. Laser-driven fuel injection for deep penetration fueling in TIBER.

pressure n_0T_0 and forward dynamic pressure $1/2(n_0/m_i)v_E^2$ both exceed the local magnetic field pressure $B^2/2\mu_0$ by many orders of magnitude, and so the pellet plasma trajectory is unaffected by the magnetic field initially. Thus, the penetration mechanism of this pellet plasma scheme is entirely mechanical, and not limited at all by either the strength of DT ice or the ice ablation rates of conventional pellet schemes.

Pumped Limiter

We have considered a pumped limiter as a means of conserving space in TIBER. This requires a compromise between the space available for neutron shielding of the magnets and the space needed for recycling the edge plasma. The limiter plates in TIBER are similar to those in the plasma halo dump in MARS[4] and are sized and contoured to handle the heat load without regard to gas removal. Then small pumping ports that remove the gas through the plates are located as needed to control the amount of recycling. In the case of a pumped limiter, this vented-port concept has the additional advantage of moving the leading edge out of the plasma to where heat and erosion problems are minimized. Figure 2 shows a sketch of a pumped limiter using this concept. Each small port has its own leading edge, but the large area surrounding allows adequate cooling. The peak-surface heat load is 2 MW/m^2 and the average is 1.25 MW/m^2.

Because of the toroidal magnetic field, the plasma contacts the dump plates at grazing incidence and cannot stream through the small ports. Gas is removed through the ports when the gas pressure on the plasma side of the plates exceeds that in the pumping duct behind the plates. This sets an upper limit on the gas pressure in the duct, but this limit is rather high. When the recycling fraction of the edge plasma is sufficient to protect the dump plates, the gas pressure on the plasma side is nearly equal to the plasma pressure (about 0.1 Torr). It should be possible to obtain a pressure of a few tens of millitorr in the duct, which would allow mechanical pumps to remove the gas. The duct space behind the plates can be thin, 4 cm maximum, because of the high pressure and because the duct space extends completely around the torus.

One 0.19-m-diameter vacuum pipe at the top and one at the bottom pass between each of the TF coils. The shielding displaced by these pipes is located between the coils, so that the neutron flux to the coils is only increased slightly.

Nuclear Heating of TF Coils

Estimates of nuclear heating in the TF coils for three cases are given in Fig. 3, in which the major radius and the mode of plasma removal (divertor or pumped limiter) are varied. These estimates are based on 1-D slab-shielding calculations applied to the TIBER geometry using a generic tokamak-neutron-source distribution. The major element in the shield is tungsten, making it space efficient but expensive. Thus, it should be used only where space is limited, mainly on the inner leg.

Using this generic neutron source distribution[5] results in a peak neutron wall loading greater than 2 MW/m^2 on the outer leg. This distribution is very favorable because it allows for the possibility of a nuclear component test program at near reactor levels, even though the average wall loading is less than 1 MW/m^2. From the FINESSE Study,[6] certain groups of tests suitable for TIBER have been identified. These are:

- Structural mechanics
- Breeder/multiplier structure interaction
- Thermal hydraulics
- Tritium production
- Nuclear heating and low fluence damage
- Instrumentation and control

Magnet Designs

One of the more challenging magnet designs is the 14-T pusher coil. We used conductor designs that have been proven to be both functional and within the present manufacturing capabilities. The outer section of the pusher coil is the niobium-titanium conductor used for the MFTF yin-yang coils, and the inner niobium-tin coil like that used for the MFTF choke coil. Each coil is immersed in superfluid helium to increase its current density and stability.

The original MFTF yin-yang conductor produced a peak field of 7.8 T at 4.2 K. Reduced temperature operation at 1.8 K yields an even higher critical current in the superconductor at 10-T fields. This implies that the current in the original MFTF winding pack can be increased by 28% to satisfy the Nb-Ti background coils. The heat flux for stability in the high-field pusher is $(1.28)^2$ x 0.19 or 0.31 W/cm^2, which is manageable by He-II. Hence, the yin-yang conductor in the outer section of the pusher coil can operate at a current of 7399 A, but hoop forces must be reacted to the external case structure.

For the inner high-field section of the pusher coil, a Nb_3Sn:Ti conductor originally tested at 12.7 T for MFTF can be used with He-II in fields of 14 T because of the low temperature enhancement of J_c. However, in this application the extra copper stabilizer should be annealed for high-conductivity to limit the wetted perimeter heat fluxes to 1.0 W/cm^2. This implies that the large 335 MPa stresses must be reacted externally to prevent damage to the strain-sensitive Nb_3Sn:Ti. Since the radial pack thickness is only 12.5 cm, the coil design permits transmitting the conductor stresses to a 2-cm-thick stainless-steel outer case surrounding the Nb_3Sn:Ti subcoils. The coil assembly consists of ten subcoils each clad in 1-cm-thick coil cases in order to increase the effective coil modulus and transmit the radial compressive forces from the TF coils to the additional

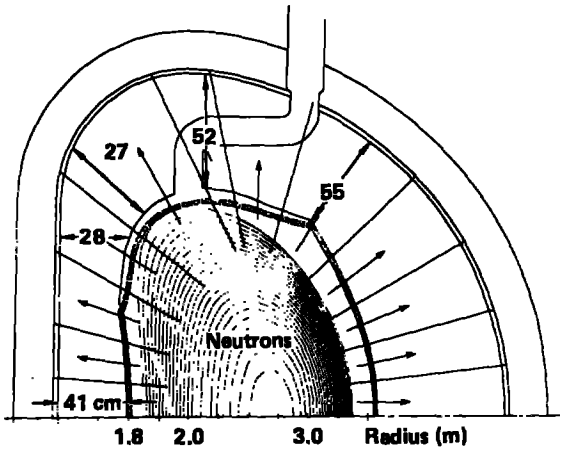

Case	P-fusion (MW)	Heating (kW)	Wall loading (MW/m^2)
1: R = 2.6 m with divertor (shown)	200	415	2.1
2: R = 2.73 m with divertor	237	96	2.3
3: R = 2.6 m with pumped limiter	200	43	2.1

Figure 3. Estimate of nuclear heating in the coils and cases and in the first wall loading at the midplane of the outer leg in TIBER.

supporting structure located at the magnet bore. The fringe fields from this coil supply an approximate 0.5 T on the plasma "bean-contour."

The TF coils summarized in Table 2 and shown in Fig. 4 for TIBER are made of internally cooled Nb_3Sn conductors similar to those used in the Westinghouse LCP coil and the MIT test coil. The tensile load on the straight leg of the TF coil has been calculated. Since the conductor loads are transmitted first to the sheath and then to the case, the sheath material shares part of the load. This sheath stress is found to be 266 MPa (39 ksi).

Cryogenic Design

In steady state, the helium liquefier required to support the entire cryogenic heat load is 50 kW, about three times the size of the system constructed for the MFTF. Nuclear heating of 43 kW in the TF coils must be removed by flowing the helium through the conductors. Because of the competing effects of heat removal and heat generation by friction, there is a minimum temperature increase in the flow path as flow rate is increased. Pancake-winding the coils, two in hand, and injecting flow on the inner layer requires 36 flow paths per coil. With an average conductor nuclear heating rate of 8.1 mW/cm^3, a flow rate of 6 kg/s is needed with inlet conditions of 6-atm pressure and 4.5 K and outlet conditions of 2 atm and 6.0 K. These parameters represent the maximum refrigeration requirements since they result from an attempt to obtain the minimum helium temperature rise. If greater temperature rise can be tolerated, less refrigeration power will be required.

The total heat to each turn of the coil and the resultant temperature at the end of the turn was calculated. This along with the field intensity was used to determine temperature margin (cryostability)

Table 2. TIBER TF-coil pack parameters.

Coil cross section (straight leg)		0.143 m^2
Winding pack cross section		.0903 m^2
Number of turns		192
Pack current density		45 A mm^{-2}
Effective area		21.67 mm^2
	% steel 25	
	% insulator 17	
	% conductor 33	
	% helium 23	

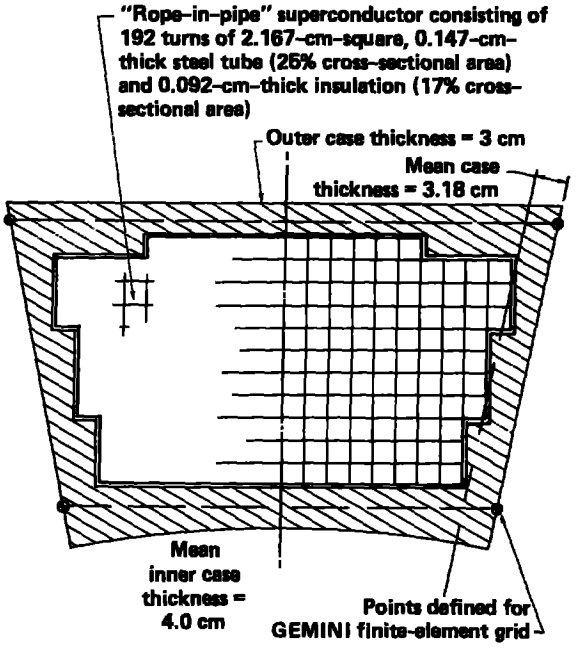

Figure 4. Toroidal field coil inboard leg, showing conductor location and case walls.

of each turn. Solving for temperature requires an iterative solution because of the strong interdependence between pressure and enthalpy. The results plotted in Fig. 5 show that the 2100 g/s flow rate maintains the coil below 6 K; conductor current sharing does not start until 7.5 K is reached. This temperature difference provides ample stability. Figure 5 is based on the following coil geometry:

Coils per machine	16
Paths per coil	20
Turns per path	12, pancake wound from coil i.d. to o.d. (turn #1 is nearest the plasma)
Flow area per path	1.14 cm^2
Hydraulic diameter	0.06 cm
Total neutron heat absorbed	43 kW

It is interesting to note that peak temperatures in the coil are not at the outlet but nearer the middle of the cryogen path. This results from relatively low heat load on the outer turns and Joule-Thompson expansion of the helium within the coil.

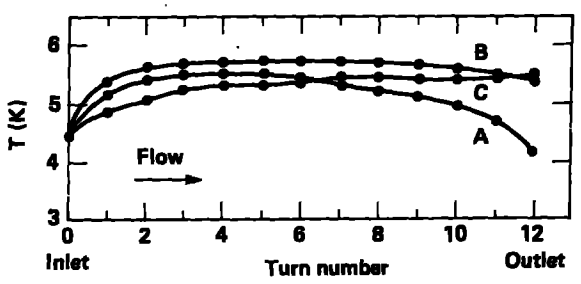

Notes	Flow (g/s)	P_{in} (atm)	P_{out} (atm)	Coil Design
A	2100	3.0	0.8	2 (12 turns/path)
B	2100	3.5	1.8	2 (12 turns/path)
C	4000	3.0	2.5	1 (6 turns/path)

Figure 5. TF coil temperature distribution.

Stress Analysis

The EFFI code was used for magnetic force analysis and combined with the GEMENI finite element code to perform stress analyses on TIBER. A radially inward force on the inboard TF coil leg creates a uniform pressure of 63.9 MPa (9,270 psi) on the small PF coils, the pusher-coil, and the spacer rings. These coils and spacer rings must be dimensioned and shimmed to make a close fit on the post. This eliminates induced shear and limits the radial stress in the post, as well as in the coil cases and spacer rings, to 63.9 MPa. If the post were not present, the tangential stress at the coil and spacer bores would be 176 MPa psi, and the induced shear would be 88 MPa.

Simple torsion calculations were made to predict approximate shear in the TF coil case at the tokamak midplane. We neglect any restraint from the top/bottom TF coil case so the stress calculated is higher than one would obtain if the whole system could be included. With a magnetic torque of 2.3×10^8 neutron-meters, the shear stress at the machine midplane was shown to be 346 MPa--a reasonable stress level for type 304 LN steel at 4.5 K.

GEMENI uses the Von Mises criteria for failure (also known as the "maximum distortion energy theory." It has gained general acceptance for both brittle and ductile materials). The effective stress (S_f) calculated for this complex array of TF coil legs, radial spacers, and post is 607 MPa. This is higher than the 460 MPa usually used for 304 LN stainless steel at a temperature of 4.5 K, but it is acceptable for Nitronic 40 and newer classes of Fe-Mn-Cr steels now being developed.[7]

The distribution of TF coil forces causes considerable variation in effective stress along the length of the inboard leg of the TF coil. We illustrate that variation in Fig. 6, where only Von Mises effective stresses are plotted. The reason that two values (S_{f+} and S_{f-}) are shown is that calculations for both sides of the plate are made (i.e., the side facing the superconductor and the side visible to an observer). The difference is small. We have plotted not only values for the TF coil case, but also those for the post and for the push coil "washers." The latter are seen to be lower than the

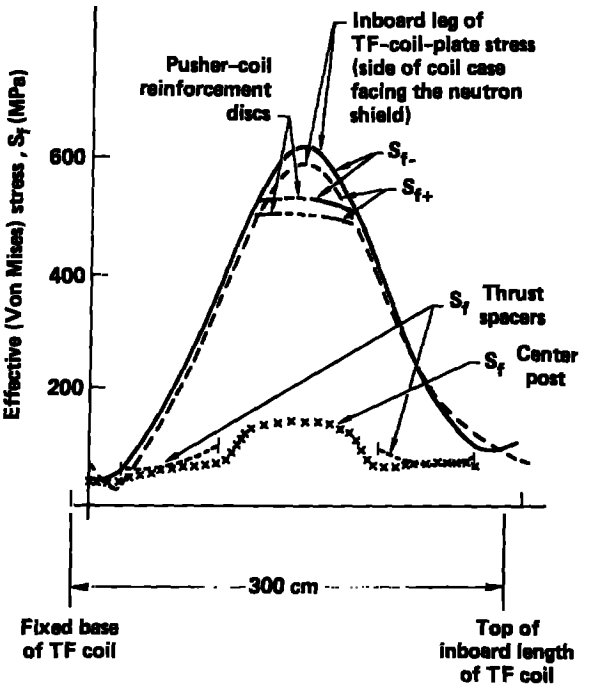

Figure 6. Von Mises stress at important points in TF coil, spacer, pusher coil, and center post.

case stresses. The S_f of 534 MPa for the pusher coil washers indicates that the number and thickness assumed is nearly optimum. There would be nine disks, each 1-cm thick, equally spaced along the length of the pusher coil.

The greatest challenge in assembling the TF coils is to join them near the center post in a manner that permits shear stresses to be transmitted between adjacent coil cases. The tendency to "overturn" is thus resisted. One solution would be to machine a number of pilot semicircular grooves in the case sides. The centerlines of the grooves must point toward the centerline of the post after all the TF coils were in position. Adjacent case sides would have mirror-image grooves and, if alignment were perfect, a pin could be inserted in the "hole" so formed. That level of precision is certainly too costly and probably impossible. Instead we would rough-machine the grooves to about 75% of their final diameter. After the TF coils were located against the post, the holes would be enlarged and reamed, using the small and mismatched grooves as a "pilot hole." Calculations of shear ndicate that 20 of the 2.5-cm-diameter dowels at each case interface would develop the needed balancing shear force at a stress level of 330 MPa. Since no other loading exists on the dowels, this should be a tolerable stress level.

Costs

The subsystem costs were either based on the methodology developed for TFCX[8], or adopted directly when we could comfortably assume equal complexity and cost for TIBER and TFCX candidate designs. The costing basis and unit quantities are shown in Table 3. A more detailed breakdown and justification

Table 3. TIBER direct costs.

Component	Cost (M$)
Project management and systems engineering	93.6
Energy and particle removal	32.3
First wall assembly	8.9
Vacuum vessel assembly	10.5
Shielding system	46.1
TF magnet system	81.0
PF magnet system	49.2
Tokamak structure	7.1
Remote maintenance	18.5
Diagnostics	41.0
LHRF system	176.9
ICRH system	0.0
ECRH system	0.0
Electric power system	72.1
Instrumentation and control system	54.1
Water cooling system	18.7
Cryogenic system	25.0
Fueling system	13.6
Vacuum pumping system	19.5
Buildings and facilities	180.0
Cleanup, disposal, and monitoring system	15.1
Total system *	963.2 M$

* Does not include contingency, escalation, or R & D costs.

for these costing elements can be found in the TFCX Preconceptual Design Report.

We did not expect a radical reduction in cost from TFCX options under the above methodology; This turned out to be the case. However, the TIBER design does promise a higher performance option for a somewhat smaller investment than any of the four versions of TFCX. Most of the savings are attributable to the more aggressive approach to the magnet design from both a current density and heating standpoint. If we were to investigate other subsystems such as the conventional facilities we could probably further reduce the total cost of TIBER.

Future Work--Improved Concepts for Steady-State Tokamaks

The TIBER concept demonstrates the possibility of an ignited, superconducting, steady-state tokamak with a major radius comparable to those of the intermediate-size, copper coil tokamaks now in operation. It was conceived as a demonstration experiment that would break the 3.0 m, and Q = 10 current drive barriers simultaneously, using design innovations to reduce the fundamental limitations of superconducting tokamaks. However, its parameter set was not selected with the aid of any searches through parameter space. Examples of mission enhancements that might be possible for a TIBER-class machine include the following:

- Entrance into the second critical beta regime. This might logically be easier to achieve in a machine that ignites at a lower beta and a higher aspect ratio.

- Steady-state operation with slow wave current drive. This would be desirable for several reasons. Slow-wave current drive is the only form of noninductive current drive that has been definitively demonstrated to exist. A plasma operating from the slow-wave then would greatly enhance the credibility of steady-state operation. Furthermore, the slow-wave has not been demonstrated to be inadequate as a reactor concept. The STARFIRE[9] study showed that Q > 30 could be achieved, if the slow-wave were absorbed near the edge of a plasma, a concept not incompatible with the current profiles of high beta plasmas.

- Steady-state operation with both slow-wave and fast-wave current drive. This concept is not merely two experiments, instead of one, but promises the best of both possible worlds. The slow wave is better for edge current drive and for low-beta, low-temperature plasmas. The fast wave is better for central absorption and for high-beta and high-temperature plasmas. A machine provided with both types of current drive would not have its mission endangered by confinement, pressure, or profiles that were significantly different from those expected. It is even conceivable, using a square wave guide, to use the same rf sources, power supplies, and transmission systems for both the slow wave and fast wave, creating any combination of the two by inserting or deleting twist guides. Finally, the unprecedented control of plasma q-profiles available with a combination of central current drive, edge current drive, and electric field would offer the best opportunity for entering the second critical beta regime without plasma indentation or for optimizing the combined beta and transport profiles in the first critical beta regime. Therefore, a useful purpose for a parametric study would be to examine whether there is any section of parameter space that would simultaneously permit fast-wave and slow-wave steady-state burn, without costing significantly more than TIBER.

Some of the improvements mentioned above[10] should be taken from the preconceptual to the conceptual level, including the strategies for combining slow wave with fast wave current drive and for using q-profile control to increase the Troyon parameter without major modifications to the first wall, shield, and TF magnets. Other improved concepts might include the use of compressional Alfven wave current drive or polarized fuel to search for a Q of 15 to 20 steady-state current drive plasma.

REFERENCES

1. C. D. Henning, E. N. C. Dalder, J. R. Miller, and L. J. Perkins, "Superconducting (Radiation Hardened) Magnets for Mirror Fusion Devices," in Proc. of IEEE 10th Symposium on Fusion Engineering, Philadelphia, PA, Dec. 1983.

2. C. F. F. Karney and N. J. Fisch, Efficiency of Current Drive by Fast Waves, Princeton Plasma Physics Laboratory, Princeton, NJ, PPPL-2128 (1984).

3. Invented by B. G. Logan.

4. B. G. Logan, C. D. Henning, G. A. Carlson, and R. W. Werner, MARS: Mirror Advanced Reactor Study, Lawrence Livermore National Laboratory, Livermore, CA, UCRL-53480 (1984).

5. D. L. Chapin and W. G. Price, Jr., Nuclear Technology 31, 32 (1976).

6. M. Abdou et al., "FINESE", UCLA ENG-84-30, Oct. 1984.

7. E. N. C. Dalder and J. W. Morris, "Cryogenic Structural Materials for Superconducting Magnets," SMIRT Vol. N, Brussels (1985).

8. TFCX Cost Specification PPPL Report A-AXXX-8406-011, June 1984.

9. C. C. Baker et al., Starfire - A Commercial Tokamak Fusion Power Plant Study, ANL/FPP-80-1, Sept. 1980.

10. J. H. Shultz, "Parametric Studies of Next Step Superconducting Tokamak Experiments at Constant Wall Loading," MIT Plasma Fusion Center Report PFC/RR-81-1, Jan. 1985.